Zero Kinetic Energy Photoelectron Spectroscopy of Benzo[*h*]quinoline

Colin Harthcock, Jie Zhang, and Wei Kong*

Department of Chemistry, Oregon State University

Corvallis, Oregon 97331

Manuscript for submission to the Journal of Physical Chemistry A, Special Issue entitled: Dynamics of Molecular Collisions XXV: Fifty Years of Chemical Reaction Dynamics, August 2, 2016

*Corresponding author, wei.kong@oregonstate.edu, 541-737-6714 (ph), 541-737-2062 (fax)

Abstract

We report zero kinetic energy (ZEKE) photoelectron spectroscopy of benzo[*h*]quinoline (B*h*Q) via resonantly enhanced multiphoton ionization (REMPI) through the first electronically excited state S_1. From the simulated REMPI spectra with and without Herzberg-Teller coupling, we conclude that vibronic coupling plays a minor but observable role in the electronic excitation to the S_1 state. We further compare the S_1 state of B*h*Q with the first two electronically excited states of phenanthrene, noticing a similarity of the S_1 state of B*h*Q with the second electronically excited state S_2 of phenanthrene. In the ZEKE spectra of B*h*Q, the vibrational frequencies of the cationic state D_0 are consistently higher than those of the intermediate neutral state, indicating enhanced bonding upon ionization. The sparse ZEKE spectra, compared with the spectrum of phenanthrene containing rich vibronic activities, further imply that the nitrogen atom has attenuated the structural change between S_1 and D_0 states. We speculate that the nitrogen atom can withdraw an electron in the S_1 state and donate an electron in the D_0 state, thereby minimizing the structural change during ionization. The origin of the first electronically excited state is determined to be 29410 ± 5 cm^{-1} and the adiabatic ionization potential is determined to be 65064 ± 7 cm^{-1}.

Key words: zero kinetic energy photoelectron spectroscopy, resonantly enhanced multiphoton ionization, benzo[*h*]quinoline, polycyclic aromatic hydrocarbons, far infra-red spectroscopy

Introduction

Polycyclic aromatic hydrocarbons (PAHs) consist of fused benzene rings without any heteroatoms and with characteristic delocalized π electrons. When one or more nitrogen atoms are included in the molecular frame, the resulting molecule is denoted as PANH. Spectroscopy of PAHs and PANHs is not only interesting from a fundamental point of view, but also of practical value in the fields of astrophysics and astrobiology.[1-4] Infrared (IR) and far-infrared (FIR) bands have been observed to emanate from deep space since the 1970s and more recently by the Herschel Space Telescope and the Stratospheric Observatory for Infrared Astronomy.[2,5-11] These ubiquitous unidentified infrared bands (UIB) are thought to contain spectroscopic signatures of molecules that constitute the interstellar medium (ISM), hence identification of these suspected molecules through spectroscopic assignments could help to determine the chemical composition of the ISM.[12,13] The close match between the UIB spectra and transitions of several functional groups of aromatic molecules alludes to the possibility of PAHs in the ISM.[2,5,7,14,15] The existence of PANHs has been postulated because of their relatively strong bands between 1000 - 1750 cm^{-1}; a region associated with the C-N-C in-plane vibrations.[16-18] The presence of stray interstellar ionizing radiations further suggests the possibility of ionized PAHs and PANHs.[7,15,19] From the perspective of astrobiology, PAHs and PANHs are of particular interest because of their potential relation to the origin of life through the formation of primitive organic molecules, including ribonucleic acids in a pre-DNA environment.[3,20] Fundamentally, comparative studies of PAHs and PANHs are also of interest in physical chemistry; nitrogen substitution into the molecular frame of a polycyclic aromatic hydrocarbon lowers the molecular symmetry and interrupts the aromaticity of the molecule.[1,19,21]

Far-infrared spectra are considered to be fingerprints for PAH species because of their sensitivity to molecular skeletal modes,[22-24] and zero kinetic energy (ZEKE) photoelectron spectroscopy offers a unique and powerful approach for obtaining frequency information of FIR bands.[25] The mid and near infrared spectral regions contain localized vibrational modes which are characteristic of specific functional groups, and experimental studies in these regions have been prolific: examples include single-photon infrared emission spectroscopy, matrix isolation spectroscopy (MIS), and cavity ringdown spectroscopy.[7,26-30] The far-infrared spectral region, on the other hand, suffers from low oscillator strength as well as other experimental difficulties, including inadequate light sources and insensitive detectors. Zero kinetic energy photoelectron spectroscopy, governed by a completely different set of selection rules from infrared spectroscopy, however, is ideal for detecting low energy vibrational modes of cations using commercially available light sources and efficient microchannel plate detectors.[31] Using ZEKE, we have studied four peri-condensed species including pyrene, benzo[*a*]pyrene, benzo[*e*]pyrene and benzo[*ghi*]perylene as well as four cata-condensed species including triphenylene, tetracene, pentacene and chrysene.[32-39] Our ZEKE data, supplemented by matrix isolation spectroscopy and other excitation and fluorescence spectroscopy,[7,26-30] allow for a comprehensive analysis of the vibrational states of cationic PAHs. These experimental results can further benchmark theoretical calculations and astrophysical modeling.[40,41]

In this work, we report resonantly enhanced multi-photon ionization (REMPI) spectroscopy of the first electronically excited state S_1 as well as ZEKE spectroscopy of the cationic state D_0 of benzo[*h*]quinoline (B*h*Q). We compare the spectroscopic features of B*h*Q with those of two isoelectronic systems phenanthrene and anthracene, and comment on the unique contribution of the nitrogen atom.[16,18,42-46] We observe that in terms of molecular orbitals, the first two electronic states of B*h*Q are in reverse order relative to those of phenanthrene, a not-so-subtle effect of the heteroatom in the molecular frame.[44-47] The low molecular symmetry has relaxed the selection rule in vibronic transitions, allowing all in-plane modes to be observable. Nevertheless, the ZEKE spectra are sparse, implying structural similarities between the cation and the first excited electronic state. We also notice a consistent increase in the vibrational frequencies of several observed modes in the D_0 state compared with those from the S_1 state, an indication of increased aromaticity upon ionization.

Experimental Setup and Calculation Method

The experimental apparatus consisted of a differentially pumped molecular beam apparatus with the detection chamber enclosed inside the source chamber, as detailed in several of our previous publications.[32-39] A time-of-flight mass spectrometer in the detection chamber also served as the pulsed field ionization zero kinetic energy spectrometer. Benzo[*h*]quinoline (Aldrich) was housed and heated to 84°C in a pulsed valve (Parker Finnegan, Series 9) with a 1 mm orifice located in the source chamber. The sample vapor was seeded in 1700 Torr of argon and co-expanded into vacuum through the pulsed valve. The sample beam was further collimated by passing through a 2 mm skimmer before reaching the detection chamber for laser excitation and ionization. The laser system for the REMPI experiment included a Nd:YAG (Spectra Physics, GCR 190) pumped dye laser (Laser Analytical System, LDL 20505) equipped with a frequency doubler for excitation and an optical parametric oscillator (Continuum, Panther, pumped by Precision I 8000) for ionization. The excitation laser in the 322.5 - 342.6 nm range had a typical pulse energy of ~1 mJ/pulse with a bandwidth of 0.5 cm^{-1}. The ionization laser in the 273 - 281 nm range had a pulse energy of ~0.5 mJ/pulse with a bandwidth of 0.3 cm^{-1}. The absolute wavelengths of both lasers were calibrated using an iron hollow-cathode lamp filled with neon based on values from the National Institute of Standards and Technology. The excitation and ionization lasers were set to counter-propagate, and the light path, the flight tube, and the molecular beam were mutually perpendicular. Two delay generators (Stanford Research, DG 535) controlled the timing of the lasers, and the optimal signal was obtained via temporal and spatial overlap of the two lasers. In the ZEKE experiment, molecules were excited to high Rydberg states for 400 ns in the presence of a constant DC spoiling field (below 50 mV/cm), after which ionization and extraction were achieved by a pulsed electric field of 2 V/cm.

The Gaussian 09 suite[48] was used to optimize the molecular structure, to obtain frequencies from the optimized molecular frame and to simulate the observed vibrational structures from the REMPI and ZEKE experiments. For the ground state of the neutral and cationic state, density functional theory (DFT) calculations using the B3LYP functional were performed with the 6-31G basis set. The S_1 and S_2 electronically excited states were calculated using time dependent density functional theory (TD-DFT) with the B3LYP functional and the 6-31G basis set. Further details of the calculation will be provided in the following section.

Results

Two-color 1+1' REMPI spectroscopy

The two-color 1+1' REMPI spectroscopy of benzo[*h*]quinoline near the origin of the $S_1 \leftarrow S_0$ electronic transition is displayed in Figure 1. The ionization laser was set at 280 nm and was temporally and spatially overlapped with the scanning resonant laser. After each laser shot, a complete time-of-flight mass spectrum could be observed, and clear presence of intact molecular ions of B*h*Q could be identified as the excitation laser was scanned through the recorded spectral region. Other than the appearing and disappearing parent ion with wavelength, the mass spectrum contained no sign of molecular clusters or other impurities. We briefly varied the stagnation pressure and the heating temperature of the sample, with no effect on the resulting mass spectrum, further eliminating the possible contribution of molecular clusters. Each data point was an average of over 100 laser shots, and the spectrum was repeated over a period of three months. The band second to the lowest energy transition at 29410 ± 5 cm^{-1} was assigned as the origin and was the second most intense in the spectrum. The assignment for the lowest energy transition as a hot band of $(1a")^2$ was based on two considerations. First, by improving the cooling condition of the supersonic molecular beam, we were able to lower the intensity of the putative hot band, and second, the simulated REMPI spectrum agreed with the current assignment (see Fig. 2).

Table I lists the frequencies of the observed vibrational bands, frequencies from the calculation, and spectroscopic assignments. The vibrational frequencies were calculated using TDDFT at the B3LYP/6-31G level. Based on our current assignment and using the least-squares fitting procedure, we obtained a scaling factor of 0.963 for the calculated frequency with a coefficient of determination of 0.9998. The experimental data were limited by the linewidth of each band, which resulted in an uncertainty of 5 cm^{-1}.

The first two electronically excited states of B*h*Q are closely spaced in energy, and the proximity can be a source of confusion for the DFT calculation.[32-38,48] We simulated the excitation spectra to both the putative S_1 and S_2 electronic states, and to further illustrate the effect of Herzberg-Teller (HT) vibronic coupling, we also calculated a spectrum containing only the Franck-Condon factor for the vibronic bands to the S_1 state. The calculation results are shown in Fig. 2 for comparison with the experimental data. The similarity between panels (c) and (d) confirms the assignment of the $S_1 \leftarrow S_0$ transition. Moreover, HT coupling introduces few new vibrational modes; rather the intensities of some vibronic bands, in particular, the 7a' band, are visibly enhanced.

The agreement between simulation and experiment can further assist with spectral assignment. For example, the band at 446 cm^{-1} has a deviation of 11 cm^{-1} from the calculation, but because of its presence in the simulated spectrum, we are comfortable in its identity as the 3a' band. A similar situation exists for the band at 1208 cm^{-1} (19a'). The experimental spectrum contains several clusters of congested transitions above 700 cm^{-1}. Although the calculation has reproduced some of the clusters of transitions, the density of transitions from the calculation is still below that of the experiment. Consequently, assignment within each cluster is difficult and tentative, and some unusually large deviations are noticeable. Moreover, the transition at 409 cm^{-1} is clearly missing in the calculation. Our tentative assignment of a combination band 3a"4a" is based on possible combinations of low frequency bands and the selection rule for vibronic transitions. The assignment of this band will be discussed again in the ZEKE experiment. Overall mostly in-plane vibrational modes can be observed, for example, the 2a' mode involving elongation along the long axis and the 7a' mode corresponding to breathing of the molecular frame.

The observed vibronic distribution of Fig. 1 is largely similar to the fluorescence excitation spectrum reported by Prochorow, Deperasińska and Stepanenko (PDS).[49] However, the spectrum of the PDS report contains two bands below the strongest band at 29409 cm^{-1}, and the lowest energy band at 29226 cm^{-1} is considered the origin band. If we revise the PDS assignment by shifting all vibronic bands by 184 cm^{-1}, the reported vibrational frequencies agree with our result within our uncertainty. Unfortunately, there is no symmetry assignment associated with the PDS report and hence no direct comparisons can be made.

ZEKE Spectroscopy

By scanning the ionization laser while setting the resonant laser at one of the intermediate states identified in the REMPI experiment, we obtained pulsed field ionization ZEKE spectra as shown in Figure 3. Similar to the REMPI spectrum, the ZEKE spectra were obtained with about 100 laser pulses per data point over a three month period. The ZEKE experiment was only successful with a few intermediate vibronic states that had relatively strong intensities in the REMPI spectrum and had internal vibrational energies below 710 cm^{-1}. The vibrational identity of the intermediate state for each ZEKE spectrum is labeled in Figure 3 with a black dot. The theoretical vibrational frequencies were calculated using DFT at the B3LYP/6-31G level, and a least-squares fitting procedure, similar to that used in the REMPI experiment, was used to obtain a scaling factor of 0.961 with a coefficient of determination of 0.9983. Table II lists the observed transitions, the corresponding theoretical values, and the assignment. The experimental uncertainty of 7 cm^{-1} is restricted by the uncertainty of the intermediate state, the linewidth of the lasers, and the pulsed electric field for ionization.

Panel a in Figure 3 contains the ZEKE spectrum recorded from the origin of the first electronically excited state, and the calculated spectrum is overlaid with the experimental data in grey based on the Franck-Condon factors of the electronic transition $D_0 \leftarrow S_1$. Once again the calculation has captured the essence of the experimental spectrum, with a predominant origin and a few much weaker vibrational bands, particularly the 7a’ band corresponding to the breathing mode of the whole molecular frame. The adiabatic ionization threshold of B*h*Q is thus determined to be 65064 ± 7 cm^{-1} (8.067 ± 0.001 eV) after taking into consideration the effect of the ionization field. This value is approximately 200 cm^{-1} higher than that from the photoelectron spectroscopy study conducted by Hush, Cheung and Hilton (8.04 ± 0.02 eV), and our value represents more than an order of magnitude increase in precision.[50]

All panels in Fig. 3 are characteristically sparse, containing primarily the band corresponding to the same vibrational excitation of the intermediate state. The 7a' breathing mode is present in four out of the six spectra as a combination with the predominant vibrational band. Panel c was obtained via the 3a"4a" intermediate level and the observed ZEKE transition was assigned as 3a"4a" in keeping with the propensity rule,[32-39] although just from vibrational frequency and selection rule points of view, the observed strongest transition could be assigned as $(4a")^2$ at 470 cm^{-1}. The weaker transition in panel f was also assigned as a combination band of two out-of-plane modes because the next nearest in-plane vibration was at 837 cm^{-1}, 30 cm^{-1} above the observed transition.

Discussion

Nature of the S_1 State

Aromaticity leads to degenerate or near degenerate molecular orbitals, which can produce closely spaced excited electronic states. With the introduction of a nitrogen atom in B*h*Q, reorganization of the nearly degenerate electronic states can be expected. Based on our calculation, the majority of the oscillator strength (60%) of the $S_1 \leftarrow S_0$ transition is derived from the transition between the highest occupied molecular orbital to the lowest unoccupied molecular orbital (the LUMO ← HOMO transition), and it is $\pi\pi^*$ in character. The resulting change in the molecular frame is elongation along the long axis by 0.04 Å (0.5%) and contraction along the short axis by 0.02 Å (0.5%). In contrast, for phenanthrene, an isoelectronic and structural analogue of B*h*Q, the first electronic transition is a mixture of transitions involving LUMO ←

HOMO - 1 and LUMO + 1 ← HOMO, while the second electronic transition is LUMO ← HOMO.[46] Based on our calculation, the molecular frame of the S_1 state of phenanthrene exhibits elongation along the long axis by 0.6% and minimal change along the short axis (0.05%), while that of the S_2 state has an elongated molecular frame by 0.06 Ȧ (0.8%) along the long axis and a contracted frame by 0.03 Ȧ (0.7%) along the short axis. The similarity in the structural change and in the nature of electronic transitions both testify to the correlation between the two electronic states of the two molecular systems, i. e., the S_1 state of B*h*Q corresponds to the S_2 state of phenanthrene.

The elongation along the long axis and the contraction along the short axis of the frame dimension account for the activities of the stretching mode 2a’ and the breathing mode 7a’ in the REMPI spectrum of B*h*Q. Comparable modes and frequencies have also been observed in the study of phenanthrene,[44] although for phenanthrene, the vibrational frequencies for both the S_1 and the S_2 states are similar. It appears that while the introduction of a nitrogen atom into the molecular frame affects the nature of electronic states, it has little effect on the bond strength and thereby the vibrational frequencies of the molecule.

This effect of the nitrogen atom on the nature of the electronic state has also been reported previously.[47] Yi, Alvarez-Valierra and Pratt have studied the electronic transitions of fluorene and its nitrogen and oxygen substituted analogues carbazole and dibenzofuran.[47] The authors have concluded that the introduction of a heteroatom causes the transition moment of the first electronic excitation to rotate by 90° relative to that of fluorene. This rotation is a direct result of reordering of the closely spaced molecular orbitals and related transitions, similar to the case of B*h*Q. The authors have further observed, as we do here, that the overall geometry of the molecular system is minimally affected by the introduction of a heteroatom in the ground state.

Nature and vibrational spectroscopy of the D_0 state

Based on our calculation, the optimized structure of the cationic state of B*h*Q shows further contraction along the short axis compared with the first electronically excited state, by about 0.5%, while the dimension along the long axis remains unchanged. This progressive shortening of the short axis from S_0 to S_1 to D_0 is unique to B*h*Q since for all the PAHs we have observed previously, the structures of S_0 and D_0 are similar while that of S_1 is distorted.[32-39] Nevertheless, the degree of change upon ionization is still low enough that a propensity of preserving the vibrational excitation of the intermediate state is still observable in Fig. 3 for all ZEKE spectra.

While the states D_0 and S_1 may be structurally similar, there is a notable difference in the vibrational frequencies, possibly denoting a difference in the bond strength or rigidity of the two states. Almost all observed vibrational frequencies for the D_0 state, with the exception of the 2a' mode, are blue shifted from those of the S_1 state, as shown in Table III. An increase in out-of-plane vibrational frequencies implies an increase in planar rigidity, a trait that is directly correlated to aromaticity.

Compared with the mass analyzed threshold ionization (MATI) spectroscopy of phenanthrene reported by Piest *et al*, the ZEKE spectra of B*h*Q are much sparser.[43] Although the MATI spectrum from the origin of the S_1 state of phenanthrene also contains a predominant origin band, many more low frequency bands have been reported, with three particularly strong features centering at 240, 550, and 700 cm^{-1}, and some out-of-plane modes.[43] Using DFT at the B3LYP/6-31G level and based on the Franck-Condon factor from S_1 to D_0, we have qualitatively reproduced the vibronic activities in the MATI/ZEKE spectrum of phenanthrene from the origin of the S_1 state. For comparison, we have also calculated the MATI/ZEKE spectrum of phenanthrene from the origin of the S_2 state. Different vibronic bands in the resulting spectra are observed from the two different electronic states, but both spectra show similar levels of vibronic activities. In contrast, the ZEKE spectrum of B*h*Q contains essentially only one in-plane vibrational band of 7a'.

The difference in vibronic structures of the ZEKE/MATI spectra between B*h*Q and phenanthrene is intriguing. Our group has investigated the ZEKE spectroscopy of a series of benzene derivatives via resonantly enhanced multiphoton ionization.[51-54] In all cases, we have discovered that the electron rich substituent attenuates the geometric change from S_1 to D_0, resulting in a vibronically active REMPI spectrum but sparse ZEKE spectra. In the MATI experiment of pyridine through REMPI,[55] with the exception of one spectrum obtained through an out-of-plane mode, all other spectra follow the propensity rule. These results are in direct contrast to the ZEKE spectrum of benzene where extensive vibrational progressions have been reported.[56] It seems that the nitrogen atom in B*h*Q has a similar effect as the substituent in the benzene derivatives and pyridine, maintaining the molecular frame during ionization from S_1 to D_0.

Our assessment of the effect of the nitrogen atom in the S_1 and D_0 states of B*h*Q has been implied in the literature.[16-18,21] Several groups have investigated the cationic ground state of B*h*Q using matrix isolation spectroscopy and infrared multiphoton dissociation (IRMPD).[16,18] The work of Mattioda *et al.* using MIS has revealed that PANHs does not present new signature vibrational bands, but rather, some transitions in the region of 1100 - 1600 cm^{-1} and 500 - 600 cm^{-1} are enhanced, corresponding to the C-C and C-N stretching, C-N-C in-plane bending, and C-N-C out-of-plane vibrational modes.[17] Using a free electron laser for multiphoton dissociation, Galue *et al.* have discovered enhanced vibrational activities in the same region of cationic PANHs, although many bands from their IRMPD experiment are red-shifted due to vibrational anharmonicity.[18] Based on these enhancement effects, Mattioda *et al.* have made an interesting observation that "the nitrogen atom in the aromatic network of the PANHs produces a pseudo-ionization effect."[17] Incidentally, the ZEKE spectra of anthracene, an isomer of phenanthrene without the kink in the structure, defy the propensity rule and contain a vibrational progression.[27]

A plausible interpretation of the effect of the nitrogen atom can be glimpsed from the charge distribution among the relevant electronic states. Based on the Mulliken population analysis from our calculation, the $S_1 \leftarrow S_0$ transition increases the negative charge on the nitrogen atom from -0.41 to -0.46 electron, and shifts ~ 0.1 electron from the farthest ring to the nitrogen containing ring. Upon ionization, on the other hand, the nitrogen containing ring loses 0.44 electron, while the farthest ring loses 0.35 electron. We therefore speculate that the stabilizing effect of the nitrogen atom comes from its electron withdrawing effect in the S_1 state and its electron donating ability in the D_0 state. Thus electron rich and electronegative substituents can buffer the geometric change from S_1 and D_0 by modifying the S_1 state to be more like the ionic state, and by modifying the D_0 state to be more like the S_1 state.

Conclusion

The vibrational characteristics of the first electronically excited state and the ground cationic state were studied using 1+1' two-color REMPI and two-color ZEKE spectroscopic techniques. The closely spaced excited electronic states of aromatic systems could easily be switched in order by the addition of a heteroatom, which was the case when we compare B*h*Q and its isoelectronic system phenanthrene. Using DFT at the B3LYP/6-31G level, we were able to qualitatively reproduce the observed REMPI spectrum and assign the vibrational bands. The ZEKE spectra obtained from a few intermediate vibronic states were sparse, following the propensity of preserving the vibrational excitation of the intermediate state. However, the vibrational frequencies of the cation were all higher than those of the S_1 state, implying stronger bonding in the cationic state. From comparisons between the MATI spectrum of phenanthrene and the ZEKE spectra of B*h*Q, we believe that similar to the case of electron rich substituents of benzene,[51-54] the nitrogen atom has played an important role in the bonding of both S_1 and D_0 states, resulting in the extra geometrical stability upon ionization. This is in contrast to the ZEKE or MATI spectra of phenanthrene and anthracene, where neither show strong propensity in vibrational distribution.

Acknowledgments

This work is supported by the National Aeronautics and Space Administration under award No. NNX09AC03G.

Figure Captions

Figure 1. REMPI spectrum of benzo[*h*]quinoline shifted by 29410 cm^{-1}. The peak observed at -183 cm^{-1} is assigned as a hot band based on simulations and experimental observations. The molecular structure with designations of axes is also included.

Figure 2. Comparison between the experimental REMPI spectrum from Fig. 1 and simulation using DFT at the B3LYP/6-31G level, with and without Herzberg-Teller coupling.

Figure 3. Experimental ZEKE spectra from a few selected intermediate vibronic states: (a) origin, (b) 2a’, (c) 3a”4a”, (d) 6a’, (e) 7a’ and (f) 8a’. All spectra are shifted by the adiabatic ionization threshold of 65064 cm^{-1}. Modes marked with a black dot are the correlated modes of the intermediate state.

Table I. Observed vibrational bands for the S_1 (A’) state of benzo[*h*]quinoline. Bands in bold-faced italic font are intermediate states which have yielded ZEKE spectra (units: cm^{-1}, uncertainty: ± 5 cm^{-1}).

Experimental	Calculation†	Assignment
-185	-204*	1a”^{2}
230	223	1a’
307	308	1a”4a”
395	***394***	***2a’***
399	400	3a”^{2}
409	***416***	***3a”4a”***
446	435	3a’
492	488	4a’
521	521	5a’
584	***586***	***6a’***
669	***674***	***7a’***
705	***700***	***8a’***
709	711	1a’4a’
720	719	5a”^{2}
733	737	5a”6a”
797	788	2a’^{2}
834	835	9a’
841	849	10a’
846	843	5a”8a”
872	870	3a’^{2}
937	936	2a”15a”
973	980	2a’6a’
1011	1010	12a’
1021	1021	3a’6a’

1028	1010	4a’5a’
1034	1037	13a’
1061	1068	2a’7a’
1075	1089	15a’
1115	1110	3a’7a’
1208	1193	19a’
1322	1327	23a’
1335	1338	7a’^{2}
1365	1363	24a’
1375	1376	7a’8a’
1390	1378	25a’
1392	1392	3a’^{2}5a’
1395	1396	26a’
1407	1416	27a’
1416	1415	1a’19a’
1438	1441	29a’
1459	1452	30a’
1493	1498	32a’
1507	1506	33a’
1510	1509	7a’9a’
1515	1502	2a’16a’
1518	1512	13a”^{2}
1525	1527	34a’

† Including a scaling factor of 0.963.

* Including the scaling factor of 0.961 obtained for the cationic ground state D_0.

Table II. Observed vibrational transitions of the D_0 state of benzo[*h*]quinoline from several intermediate vibronic transitions. The bands in bold-faced italic font are the correlated diagonal bands of the intermediate state (units: cm^{-1}, uncertainty: ± 7 cm^{-1}).

Origin	2a’	3a”4a”	6a’	7a’	8a’	Calc†	Assignment
	395					395	2a’
		477				447	3a”4a”
			600			604	6a’
688				***700***		692	7a’
					719	712	8a’
					807	787	5a”6a”
	1075					1087	2a’7a’
			1281			1296	6a’7a’
				1383		1384	7a’^{2}

† Including a scaling factor of 0.961

Table III. Frequencies of several observed vibrational modes in the cationic state D_0 and the first electronically excited state S_1 of benzo[*h*]quinoline (units: cm^{-1}, uncertainty: ± 7 cm^{-1})

Mode	S_1	D_0	$D_0 - S_1$
2a’	395	395	0
3a”4a”	409	477	68
6a’	584	600	16
7a’	669	700	31
8a’	705	719	14
5a”6a”	733	807	74

References

(1) Doerr, F.; Gropper, H.; Mika, N. The Polarization of the Π-Π Phosphorescence of N-Heterocyclics on Excitation in the N-Π Band: Quinoxaline, 2,3-Dimethylquinoxaline, Quinazoline, Benzoquinoxaline. *Ber. Bunsen-Ges.* **1962**, *67*, 202-205.

(2) Allamandola, L. J.; Tielens, A. G. G. M.; Barker, J. R. Polycyclic Aromatic Hydrocarbons and the Unidentified Infrared Emission Bands: Auto Exhaust Along the Milky Way! *Astrophys. J.* **1985**, *290*, L25-L28.

(3) Bernstein, M. P.; Dworkin, J. P.; Sandford, S. A.; Cooper, G. W.; Allamandola, L. J. Racemic Amino Acids from the Ultraviolet Photolysis of Interstellar Ice Analogues. *Nature* **2002**, *416*, 401-403.

(4) Li, A.; Lunine, J. I. Modeling the Infrared Emission from the Hd 141569a Disk. *Astrophys. J.* **2003**, *594*, 987-1010.

(5) Leger, A.; Puget, J. L. Identification of the "Unidentified" Ir Emission Features of Interstellar Dust? *Astron. Astrophys.* **1984**, *137*, L5-L8.

(6) Allamandola, L. J.; Tielens, A. G. G. M.; Barker, J. R. Infrared Emission from Interstellar Pahs. *NATO ASI Ser., Ser. C* **1987**, *210*, 305-331.

(7) Szczepanski, J.; Vala, M. Infrared Frequencies and Intensities for Astrophysically Important Polycyclic Aromatic Hydrocarbon Cations. *Astrophys. J.* **1993**, *414*, 646-655.

(8) Salama, F. Molecular Spectroscopy in Astrophysics: The Case of Polycyclic Aromatic Hydrocarbons. *J. Mol. Struct.* **2001**, *563-564*, 19-26.

(9) Mulas, G.; Malloci, G.; Benvenuti, P. Testing the "Strong" Pahs Hypothesis. Ii. A. Quantitative Link between Dibs and Far-Ir Emission Features. *Astron. Astrophys.* **2003**, *410*, 639-648.

(10) Gehrz, R. D.; Becklin, E. E.; de Buizer, J., *et al.* Status of the Stratospheric Observatory for Infrared Astronomy (Sofia). *Adv. Space Res.* **2011**, *48*, 1004-1016.

(11) Spinoglio, L.; Pereira-Santaella, M.; Dasyra, K. M.; Calzoletti, L.; Malkan, M. A.; Tommasin, S.; Busquet, G. Far-Infrared Line Spectra of Seyfert Galaxies from the Herschel-Pacs Spectrometer. *Astrophys. J.* **2015**, *799*, 1-20.

(12) Gredel, R.; Carpentier, Y.; Rouille, G.; Steglich, M.; Huisken, F.; Henning, T. Abundances of Pahs in the Ism: Confronting Observations with Experimental Results. *Astron. Astrophys.* **2011**, *530*, A26/01-15.

(13) Contreras, C. S.; Ricketts, C. L.; Salama, F. Formation and Evolution of Circumstellar and Interstellar Pahs: A Laboratory Study. *EAS Publ. Ser.* **2011**, *46*, 201-207.

(14) Leger, A.; d'Hendecourt, L.; Joblin, C. Present Situation in the Identification of Polycyclic Aromatic Hydrocarbons. *Adv. Space Res.* **1993**, *13*, 473-481.

(15) Langhoff, S. R. Theoretical Infrared Spectra for Polycyclic Aromatic Hydrocarbon Neutrals, Cations, and Anions. *J. Phys. Chem.* **1996**, *100*, 2819-2841.

(16) Mattioda, A. L.; Hudgins, D. M.; Bauschlicher, C. W.; Rosi, M.; Allamandola, L. J. Infrared Spectroscopy of Matrix-Isolated Polycyclic Aromatic Compounds and Their Ions. 6. Polycyclic Aromatic Nitrogen Heterocycles. *J. Phys. Chem. A* **2003**, *107*, 1486-1498.

(17) Mattioda, A. L.; Rutter, L.; Parkhill, J.; Head-Gorgon, M.; Lee, T. J.; Allamandola, L. J. Near-Infrared Spectroscopy of Nitrogenated Polycyclic Aromatic Hydrocarbon Cations from 0.7 to 2.5 Mm. *Astrophys. J.* **2008**, *680*, 1243-1255.

(18) Galue, H. A.; Pirali, O.; Oomens, J. Gas-Phase Infrared Spectra of Cationized Nitrogen-Substituted Polycyclic Aromatic Hydrocarbons. *Astron. Astrophys.* **2010**, *517*, A15/01-15.

(19) Rhee, Y. M.; Lee, T. J.; Gudipati, M. S.; Allamandola, L. J.; Head-Gordon, M. Charged Polycyclic Aromatic Hydrocarbon Clusters and the Galactic Extended Red Emission. *Proc. Natl. Acad. Sci. U. S. A.* **2007**, *104*, 5274-5278.

(20) Shock, E. L.; Schulte, M. D. Amino-Acid Synthesis in Carbonaceous Meteorites by Aqueous Alteration of Polycyclic Aromatic Hydrocarbons. *Nature* **1990**, *343*, 728-731.

(21) Mattioda, A. L.; Hudgins, D. M.; Bauschlicher, C. W.; Allamandola, L. J.; Biemesderfer, C. D.; Rosi, M. Infrared Spectroscopy of Matrix-Isolated Polycyclic Aromatic Nitrogen Heterocycles (Panhs). *NASA Conf. Publ.* **2002**, *2002-211863*, 135-137.

(22) Zhang, K.; Guo, B.; Colarusso, P.; Bernath, P. F. Far-Infrared Emission Spectra of Selected Gas-Phase Pahs: Spectroscopic Fingerprints. *Science* **1996**, *274*, 582-583.

(23) Denissenko, M. F.; Pao, A.; Tang, M.-s.; Pfeifer, G. P. Preferential Formation of Benzo[a]Pyrene Adducts at Lung Cancer Mutational Hotspots in P53. *Science* **1996**, *274*, 430-432.

(24) Pirali, O.; Van-Oanh, N.-T.; Parneix, P.; Vervloet, M.; Brechignac, P. Far-Infrared Spectroscopy of Small Polycyclic Aromatic Hydrocarbons. *Phys. Chem. Chem. Phys.* **2006**, *8*, 3707-3714.

(25) Mueller-Dethlefs, K. Applications of Zeke Spectroscopy. *J. Electron Spectrosc. Relat. Phenom.* **1995**, *75*, 35-46.

(26) Vala, M.; Szczepanski, J.; Pauzat, F.; Parisel, O.; Talbi, D.; Ellinger, Y. Electronic and Vibrational Spectra of Matrix-Isolated Pyrene Radical Cations: Theoretical and Experimental Aspects. *J. Phys. Chem.* **1994**, *98*, 9187-9196.

(27) Cockett, M. C. R.; Kimura, K. A Study of Anthracene-Ar_n (N = 0-5) in the Ground Cationic State by Laser Threshold Photoelectron Spectroscopy: Selective Ionization of Complex Isomers Formed in the Free Jet Expansion. *J. Chem. Phys.* **1994**, *100*, 3429-3441.

(28) Hudgins, D. M.; Allamandola, L. J. Infrared Spectroscopy of Matrix-Isolated Polycyclic Aromatic Hydrocarbon Cations. 2. The Members of the Thermodynamically Most Favorable Series through Coronene. *J. Phys. Chem.* **1995**, *99*, 3033-3046.

(29) Oomens, J.; Van Roij, A. J. A.; Meijer, G.; von Helden, G. Gas-Phase Infrared Photodissociation Spectroscopy of Cationic Polyaromatic Hydrocarbons. *Astrophys. J.* **2000**, *542*, 404-410.

(30) Kim, H. S.; Wagner, D. R.; Saykally, R. J. Single Photon Infrared Emission Spectroscopy of the Gas Phase Pyrene Cation: Support for a Polycyclic Aromatic Hydrocarbon Origin of the Unidentified Infrared Emission Bands. *Phys. Rev. Lett.* **2001**, *86*, 5691-5694.

(31) Schlag, E. W. *Zeke Spectroscopy.*; Cambridge University Press: London, 1998.

(32) Zhang, J.; Pei, L.; Kong, W. Zero Kinetic Energy Photoelectron Spectroscopy of Tetracene Using Laser Desorption for Vaporization. *J. Chem. Phys.* **2008**, *128*, 104301.

(33) Zhang, J.; Han, F.; Kong, W. Zero Kinetic Energy Photoelectron Spectroscopy of Pyrene. *J. Phys. Chem. A* **2010**, *114*, 11117-11124.

(34) Zhang, J.; Han, F.; Pei, L.; Kong, W.; Li, A. Far-Infrared Spectroscopy of Cationic Polycyclic Aromatic Hydrocarbons: Zero Kinetic Energy Photoelectron Spectroscopy of Pentacene Vaporized from Laser Desorption. *Astrophys. J.* **2010**, *715*, 485-492.

(35) Zhang, J.; Harthcock, C.; Han, F.; Kong, W. Zero Kinetic Energy Photoelectron Spectroscopy of Jet Cooled Benzo[a]Pyrene from Resonantly Enhanced Multiphoton Ionization. *J. Chem. Phys.* **2011**, *135*, 244306-244307.

(36) Zhang, J.; Harthcock, C.; Kong, W. Resonantly Enhanced Multiphoton Ionization and Zero Kinetic Energy Photoelectron Spectroscopy of Chrysene: A Comparison with Tetracene. *J. Phys. Chem. A* **2012**, *116*, 7016-7022.

(37) Zhang, J.; Harthcock, C.; Kong, W. Resonantly Enhanced Multiphoton Ionization and Zero Kinetic Energy Photoelectron Spectroscopy of Benzo[*G*,*H*,*I*]Perylene. *J. Phys. Chem. A* **2012**, *116*, 1551-1557.

(38) Harthcock, C.; Zhang, J.; Kong, W. Resonantly Enhanced Multiphoton Ionization and Zero Kinetic Energy Photoelectron Spectroscopy of Benzo[E]Pyrene. *Chem. Phys. Lett.* **2013**, *556*, 23-28.

(39) Harthcock, C.; Zhang, J.; Kong, W. Zero Kinetic Energy Photoelectron Spectroscopy of Triphenylene. *J. Chem. Phys.* **2014**, *140*, 244308.

(40) Li, A., in *Deep Impact as a World Observatory Event: Synergies in Space, Time, and Wavelengh*, edited by Käufl, H. U.; Sterken, C. (Springer, Berlin, 2009), pp. 161-175.

(41) Hu, A.; Duley, W. W. Laboratory Simulation of 11-15 Mm Spectra Associated with Polycyclic Aromatic Hydrocarbon Molecules. *Astrophys. J.* **2007**, *660*, L137-L140.

(42) Norek, M.; Kozankiewicz, B.; Prochorow, J. Spectroscopy and Photophysics of Monoazaphenanthrenes. Iii. Luminescence of Phenanthridine and 7,8-Benzoquinoline in Crystalline State. *Acta Phys. Pol., A* **2004**, *106*, 77-94.

(43) Piest, J. A.; Oomens, J.; Bakker, J.; von, H. G.; Meijer, G. Vibrational Spectroscopy of Gas-Phase Neutral and Cationic Phenanthrene in Their Electronic Groundstates. *Spectrochim Acta A Mol Biomol Spectrosc* **2001**, *57*, 717-735.

(44) Ohta, N.; Baba, H. Electronic Spectra and Intramolecular Dynamics of Phenanthrene in a Supersonic Free Jet. *Mol. Phys.* **1986**, *59*, 921-939.

(45) Warren, J. A.; Hayes, J. M.; Small, G. J. Vibronic Activity in the Laser Jet Spectra of Phenanthrene. *Chem. Phys.* **1986**, *102*, 323-336.

(46) Baba, M.; Katori, T.; Kawabata, M.; Kunishige, S.; Yamanaka, T. S_1 and S_2 States of Linear and Zigzag Cata-Condensed Hydrocarbons. *J. Phys. Chem. A* **2013**, *117*, 13524-13530.

(47) Yi, J. T.; Alvarez-Valtierra, L.; Pratt, D. W. Rotationally Resolved $S_1 <\!- S_0$ Electronic Spectra of Fluorene, Carbazole, and Dibenzofuran: Evidence for Herzberg-Teller Coupling with the S_2 State. *J. Chem. Phys.* **2006**, *124*, 244302.

(48) Frisch, M. J.; Trucks, G. W.; Schlegel, H. B., *et al. Gaussian 09, Revision A. 1;* Gaussian Inc.: Wallingford, CT, 2009.

(49) Prochorow, J.; Deperasinska, I.; Stepanenko, Y. Fluorescence Excitation and Fluorescence Spectra of Jet-Cooled Phenanthridine and 7,8-Benzoquinoline. *Chem. Phys. Lett.* **2004**, *399*, 239-246.

(50) Hush, N. S.; Cheung, A. S.; Hilton, P. R. Binding Energies of Π- and Lone-Pair-Levels in Mono- and Diazaphenanthrenes and Anthracenes. Helium(He I) Photoelectron Spectroscopic Study. *J. Electron Spectrosc. Relat. Phenom.* **1975**, *7*, 385-400.

(51) He, Y.; Wu, C.; Kong, W. Zero Kinetic Energy Photoelectron Spectroscopy of P-Amino Benzoic Acid. *J. Chem. Phys.* **2004**, *121*, 3533-3539.

(52) He, Y.; Wu, C.; Kong, W. Two-Color Two-Photon Rempi and Zeke Photoelectron Spectroscopy of Jet-Cooled 2-Chloropyrimidine. *Chem. Phys. Lett.* **2004**, *391*, 38-43.

(53) He, Y.; Wu, C.; Kong, W. Resonantly Enhanced Two Photon Ionization and Zero Kinetic Energy Spectroscopy of Jet-Cooled 4-Aminopyridine. *J. Chem. Phys.* **2004**, *120*, 7497-7504.

(54) Wu, C.; He, Y.; Kong, W. Two-Color Two-Photon Rempi and Zeke Spectroscopy of Supersonically Cooled O-Aminobenzoic Acid. *Chem. Phys. Lett.* **2004**, *398*, 351-356.

(55) Riese, M.; Altug, Z.; Grotemeyer, J. Mass-Analyzed Threshold Ionization Spectroscopy of Pyridine. Structural Distortion in the First Excited State. *Phys. Chem. Chem. Phys.* **2006**, *8*, 4441-4448.

(56) Sekiya, H.; Lindner, R.; Mueller-Dethlefs, K. Rotationally Resolved Zeke Photoelectron Spectrum of Benzene. Dynamic Jahn-Teller Effect in the $N_6(E_{2g})$ Mode. *Chem. Lett.* **1993**, 485-488.

Graphic TOC

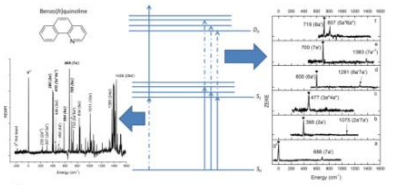
Benzo[h]quinoline
N
REMPI
Energy (cm⁻¹)
D_0
S_1
S_0
ZEKE
719 (8a')
807 (5a''6a'')
f
700 (7a')
1383 (7a'²)
e
600 (6a')
1281 (6a'7a')
d
477 (3a''4a'')
c
395 (2a')
1075 (2a'7a')
b
0⁰
686 (7a')
a
0
200
400
600
800
1000
1200
1400
1600
Energy (cm⁻¹)